Supporting Information

Designed synthesis of p-Ag_2S/n-PDI self-assembly supramolecular heterojunction for enhanced full-spectrum photocatalytic activity

Jun Yang,[a] Hong Miao,[a] Wenlu Li,[a] Huiquan Li[b] and Yongfa Zhu*[ab]

[a] *Department of Chemistry, Tsinghua University, Beijing, 100084, People's Republic of China*
[b] *Anhui Provincical Key Laboratory for Degradation and Monitoring of Pollution of the Environment, School of Chemistry and Materials Engineering, Fuyang Normal University, Fuyang 236037, P. R. China*

**Corresponding author. E-mail addresses: zhuyf@mail.tsinghua.edu.cn (Y. Zhu).*

1. Synthesis of bulk PDI

The bulk perylene diimide (bulk PDI) was synthesized by the previous work. Firstly, imidazole (18 g), perylene-3,4,9,10-tetracarboxylic dianhydride (3.5 mmol), and 3-aminopropanoic acid (28.0 mmol) were put together into a three-necked flask and heated in argon atmosphere at 110 °C for 4 h. Then ethanol (100 mL) and hydrochloric acid (2.0 M, 300 mL) were added into the flask in succession and stirred for 12 hours. And then the dark red solid was washed with deionized water until the filtrate is neutral and filtrated through a 0.22 μm filter membrane. Finally, the solid was dried at 65 °C under vacuum for 24 hours. The sample was marked as bulk PDI.

2. Photoelectrochemical measurements.

The photocurrent and electrochemical impedance spectroscopy (EIS) experiments were performed using CHI-660E electrochemical workstation. Firstly, 5 mg of catalyst was added into 1 mL of ethanol to form a uniform suspension by ultrasonic. The suspension was dropwise added to FTO glass (2 cm ×4 cm) and dried at room temperature for about 12 h. Subsequently, the FTO glass was dried in an oven at 80 ℃ for 12 hours. The FTO glass, platinum wire and a standard calomel electrode (SCE) were used as working, counter and reference electrodes, respectively. 500 W xenon lamp was used as the lightsource. Na_2SO_4 aqueous solution (0.1M) was used as the electrolyte solution.

The steady-state surface photovoltage (SPV) measurement system were performed, including a monochromatic light, a lock-in amplifier, a photovoltaic cell, and a computer. 500 W xenon lamp and a double-prism monochromator were used to provide monochromatic light. The samples were not further treated during the measurement. The contact between the indium tin oxide (ITO) electrode and materials was not ohmic. The construction of the photovoltaic cell structure is ITO-sample-ITO.

3. The photocatalytic water oxidation experiment

The full-spectrum photocatalytic water oxidation experiment was conducted with a Labsolar-IIIAG system (PerfectLight, Beijing). The photocatalyst powders (50 mg) were dispersed in 100 mL of $AgNO_3$ aqueous solution (0.01 mol·L−1) with a magnetic stirrer in a reaction cell. The silver nitrate worked as an electron acceptor. The full spectrum was obtained by a 500W xenon lamp without cuto□ filter. The gas chromatograph (GC7920, thermal conductivity detector, Ar carrier) was used for the detection of the amount of evolved oxygen.

4. Zeta potential

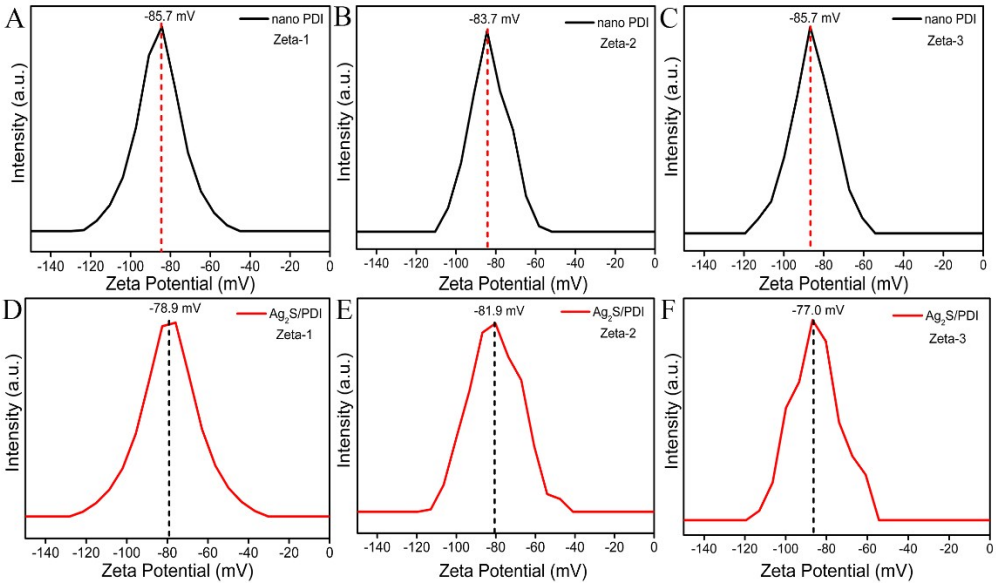

Fig. S1 Zeta potential of nano PDI (A、B、C) and Ag_2S/PDI (1:0.6, D、E、F)

Table S1. Zeta potential of PDI and Ag_2S/PDI (1:0.6).

Sample	Zeta-1	Zeta-2	Zeta-3	Zeta-average
PDI	-85.7 mV	-83.7 mV	-85.7mV	-85.0 mV
Ag_2S/PDI	-78.9 mV	-81.9 mV	-77.0 mV	-79.3 mV

As shown in Fig. S1 and Table S1, the average zeta potential ξ of PDI was -85.0 mV. Obviously, the surface of self-assembly PDI is negatively charged, positively charged silver ions (Ag^+) are easily adsorbed to the surface of the PDI via electrostatic adsorption. After adding the sulfur anion (S^{2-}), silver sulfide (Ag_2S) will be immediately formed on the surface of PDI nanowires. The average zeta potential ξ of Ag_2S/PDI was about -79.3 mV, whose surface charge becomes more positive than PDI. The change of surface charge indicates that Ag_2S successfully combines with PDI to some extent.

5. Optical band gap energies of samples

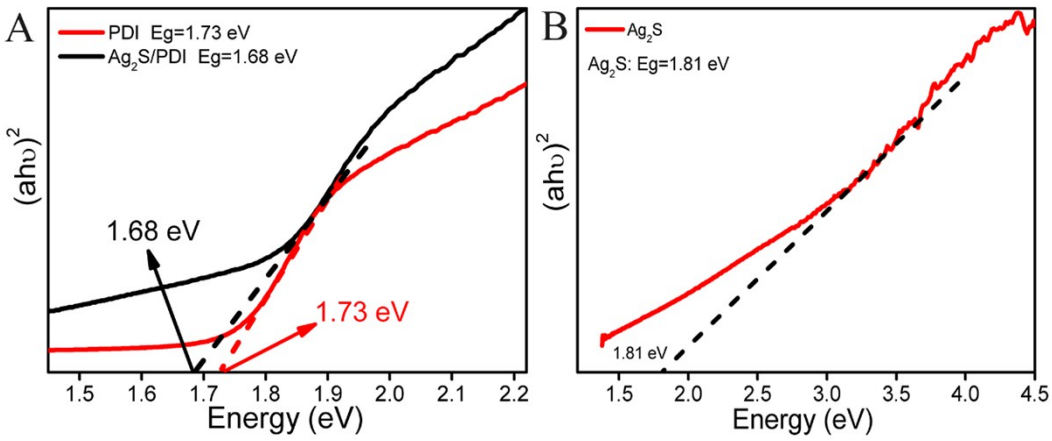

Fig. S2 Optical band gap energies of (A) bare PDI, Ag_2S/PDI and (B) Ag_2S.

Fig. S2 shows the line graph of $(ah\nu)^2$ vs. hν. The band gaps of PDI is 1.73 eV, and Ag_2S/PDI (1:0.6) is estimated to be 1.68 eV, which is narrower than that of pure PDI. Besides, the band gap energy of Ag_2S is calculated to be 1.81 eV.

6. FT-IR spectra and Raman spectra

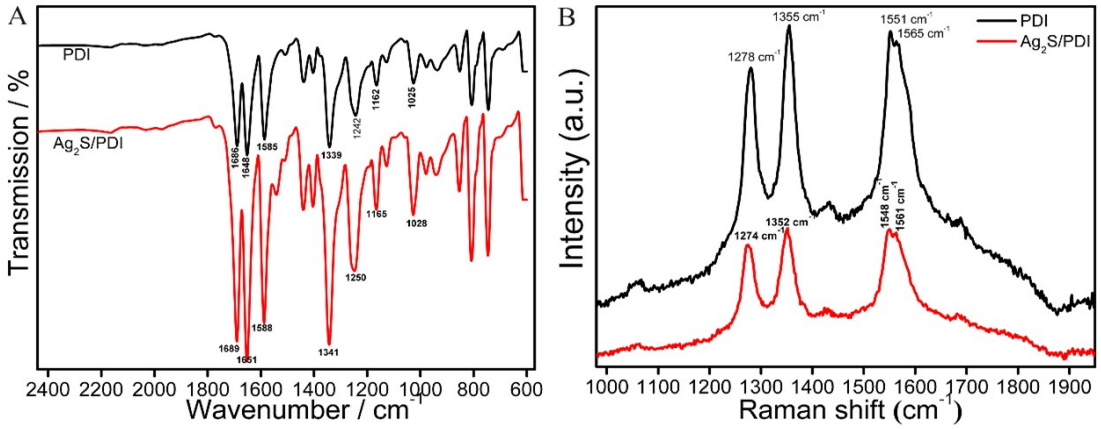

Figure S3. (A) FT-IR spectra and (B) Raman spectra of PDI and Ag_2S/PDI (1:0.6)
(1:x represents the mass ratio of Ag_2S to PDI)

To further analyze the structure of the as-prepared samples, Raman and infrared measurements were performed (Figure S3). The FTIR data of pure PDI were shown at 1648 cm^{-1} C=C and 1686 cm^{-1} C=O stretching may be attributed to the benzene ring and carboxyl structure (Fig. S3A). [1] Simultaneously, it can be clearly seen that the infrared absorption peaks of Ag_2S/PDI shifts to short wavelengths, which maybe indicate the existence of interaction between PDI and Ag_2S. The Raman spectra of PDI and Ag_2S/PDI were shown in Figure S3B. As for PDI, the peaks of 1565 cm^{-1} and 1278 cm^{-1} are respectively attributed to the stretching vibration of C=C and the CH in plane bending. [2] The intensity ratio of 1565 cm^{-1}/1278 cm^{-1} can be used to evaluate the degree of π–π stacking. [3] It

turns out that the intensity ratio of Ag_2S/PDI is 1.16, which is even higher than that of PDI (1.09), indicating that Ag_2S quantum dots promotes the degree of ordered π-π stacking, which is helpful for the long-range electrons delocalization and the migration of photo-generated electrons. The Raman spectra of Ag_2S/PDI also shows a shift compared to that of pure PDI, indicating the interaction between PDI and Ag_2S.

7. XPS spectra of Ag_2S/PDI (1:0.6) composite

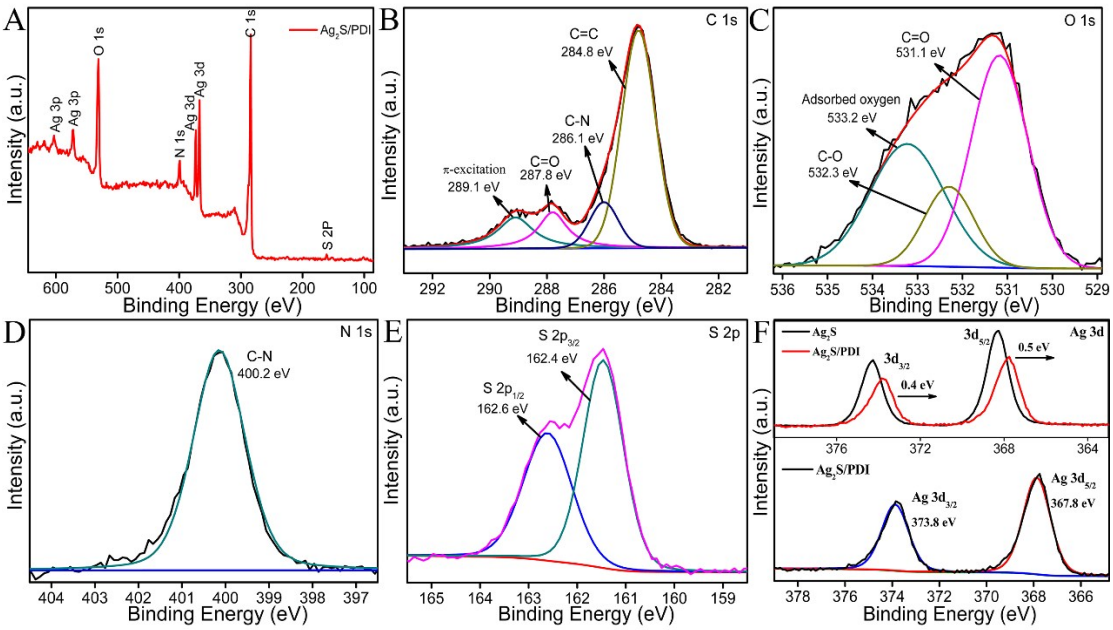

Fig. S4 XPS spectra: (A) The whole scanning XPS spectra, (B) C 1s, (C) O 1s, (D) N 1s, (E) S 2p of the Ag_2S/PDI (1:0.6) composite, and (D) the Ag 3d of the pure Ag_2S and the Ag_2S/PDI (1:0.6).

The X-ray Photoelectron Spectroscopy (XPS) of Ag_2S/PDI composite was further applied to investigate the chemical composition and surface state (Fig. S4). Figure S4 (A) shows the XPS survey spectra of Ag_2S/PDI (1:0.6) composite. It can be seen that all the peaks can be assigned to C, O, N, Ag and S elements. The narrow spectra of C 1s displayed at 284.8 eV, 286.1 eV, 287.8 eV and 289.1 eV (Figure S4 B), demonstrating the C=C, C-N, C=O and π-excitation. [4] The O 1s spectrum (Fig. S4 C) exhibited three peaks at 531.1 eV, 532.3 eV and 533.2eV, which were attributed to C=O, C-O-C and adsorbed oxygen, respectively. [5, 6] The N 1s spectrum exhibited the peaks at 400.2 eV was attributed to the C-N bond (Fig. S4 D). The S 2p spectrum exhibited two peaks at 162.4 eV and162.6 eV, corresponding to S $2p_{3/2}$, and S $2p_{1/2}$ (Fig. S4 E). Figure S4 (F) displays the high-resolution Ag 3d XPS spectra of the fresh Ag_2S/PDI (1:0.6) composite catalyst. It can be seen that two binding energy peaks appear at 367.8eV and 373.8eV corresponding to Ag $3d_{5/2}$ and Ag $3d_{3/2}$, respectively, which are attributed to Ag^+.[7] There are no XPS spectra of Ag nanocrystals existing on the surface of the composite, indicating that no Ag^0 was formed during the

preparation. In addition, the Ag 3d peak position of Ag_2S/PDI (1:0.6) is shifted toward low binding energy compared to pure Ag_2S, revealing a strong interaction between Ag_2S and PDI, which means the existence of electron transfer and chemical bonds between the two components. [8, 9]

8. HPLC spectrum

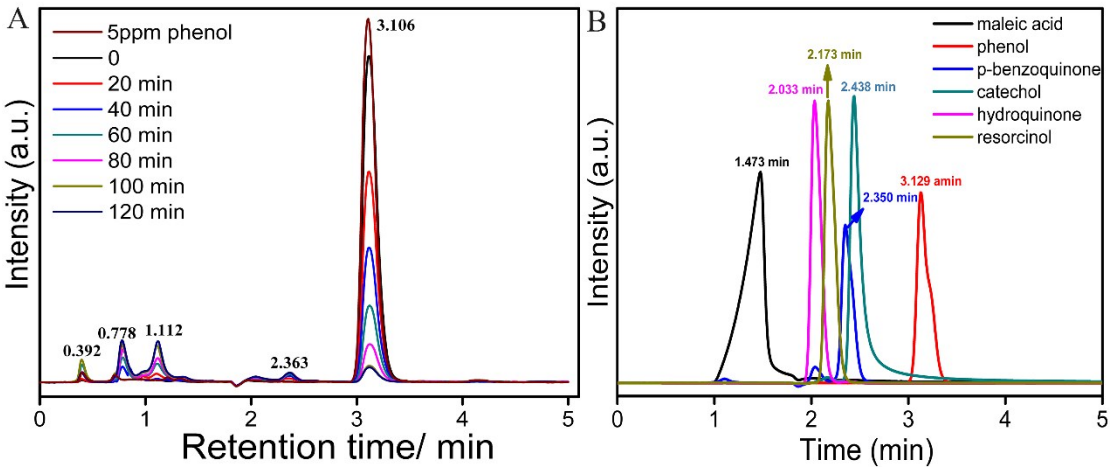

Figure S5 (A) HPLC spectrum of phenol solution degraded by Ag_2S/PDI (1:0.6) composite; (B) The HPLC spectrum of several speculated intermediate products

The HPLC (Fig. S5 A) were performed with an ultraviolet-visible detector. The peak located at 3.106 min corresponds to phenol, which is obvious that the intensity of phenol gradually decreased with continuous irradiation. Simultaneously, several speculated intermediate products were detected by HPLC (Fig. S5 B). By comparing figure S5(A) with figure S5(B), the peak of 2.363 min and 1.112 min may be attributed to p-benzoquinone and maleic acid respectively. [10] Besides, the peak of 0.392 min and 0.778 min may belong to the small molecule dissolution of nano PDI.

9. The photocatalytic degradation kinetics

The corresponding first order kinetics curve fitting of samples was shown in Figure S6. The degradation phenol process conformed to the pseudo-first-order kinetics under visible light and ultraviolet light. When the mass ratio of Ag_2S to PDI is 1:0.6, the composite exhibited the highest visible -light activity, whose apparent rate constant (0.0259 min^{-1}) is 6.93 times that of PDI (0.00374 min^{-1}). The Ag_2S/PDI (1:0.6) composite could degrade 94.48% of the phenol after visible light irradiation for 120 min. The ultraviolet-light (UV-light) photocatalytic performance of pure Ag_2S, bare PDI and Ag_2S/PDI (1:0.6) composite was shown in the Figure S6 (C) and (D). Dramatically, the Ag_2S/PDI (1:0.6) composite showed the best satisfactory photocatalytic activity of 0.0142min^{-1}, nearly 8.07 times that of pure nano-PDI (0.00176min^{-1}).

Although the p-Ag_2S/n-PDI heterojunction has been successfully formed at the interface between Ag_2S and PDI, indicating more effective separation of photon-generated carriers, excessive Ag_2S will prevent PDI from absorbing sufficient light. There is a balance between charge separation

and light absorption, where Ag_2S /PDI-1:0.6 may represent the balance point. Moderate amounts of Ag_2S can enhance the separation of photon-generated carriers, resulting in an increased catalytic activity; on the contrary, excessive amounts of Ag_2S will shade PDI, resulting in a decrease of catalytic activity.

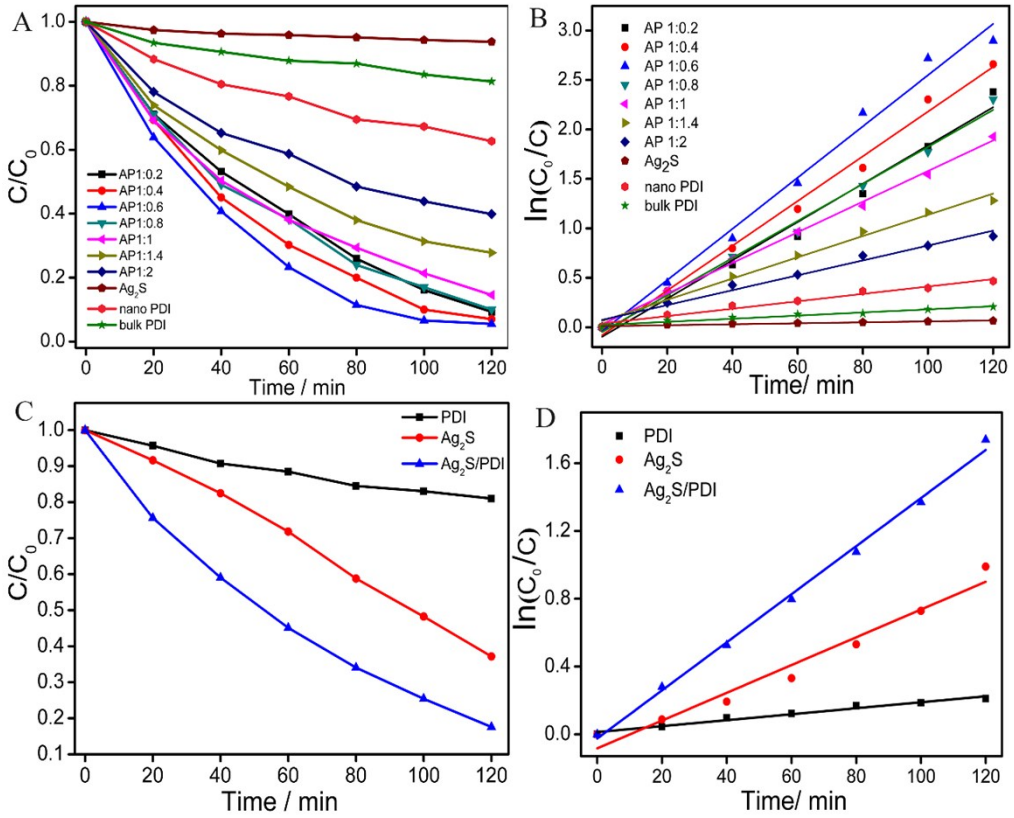

Figure S6 Photocatalytic activity curves of samples for phenol degradation (5 ppm) (A) under visible light (λ > 420 nm) and (C) under ultraviolet irradiation (254 nm); The corresponding first order kinetics curve fitting of samples (B) under visible light (λ > 420 nm) and (D) under ultraviolet irradiation (254 nm);

Table S2 Apparent rate constants *k* of several reported catalysts under visible light

Photocatalysts	Apparent rate constants k **(h^{-1})**	Reference
Bi_2WO_6	0.01614	[11]
C_3N_4	0.01456	[12]
PDI/P25	0.01000	[13]
PDI/C60	0.2160	[14]
Commercial PDI	0.09498	[10]
PDI (-COOH)	0.2244	This work
Ag_2S/PDI(1:0.6)	**1.554**	This work

The apparent rate constant of several reported photocatalysts for phenol degradation under the same conditions were listed in Table S2. The result showed that the Ag_2S/PDI heterojunction composite has the best photocatalytic performance than the photocatalysts listed in the Table S2.

10. Photocatalytic stability

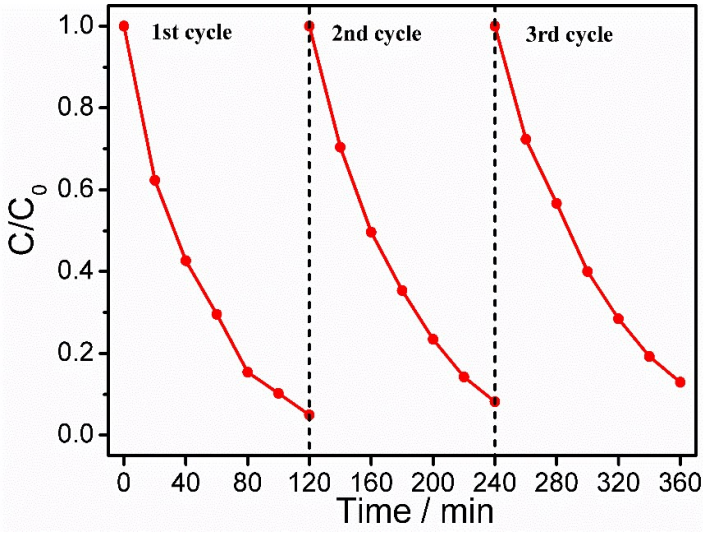

Fig. S7 Recycling tests of Ag_2S/PDI (1:0.6) for phenol degradation in the acid (pH = 4.3) environment.

The stability of photocatalysts is a critical issue in the photo-degradation reaction. As shown in Figure S7, the Ag_2S/PDI (1:0.6) composite remained high stability in acid environment (pH = 4.3). Besides, no differences have been found in the XRD spectra and FT-IR spectra of the Ag_2S/PDI (1:0.6) composite before and after catalysis at pH=6.8 (Figure S8), indicating that the molecule structure of PDI does not change during photocatalytic reaction.

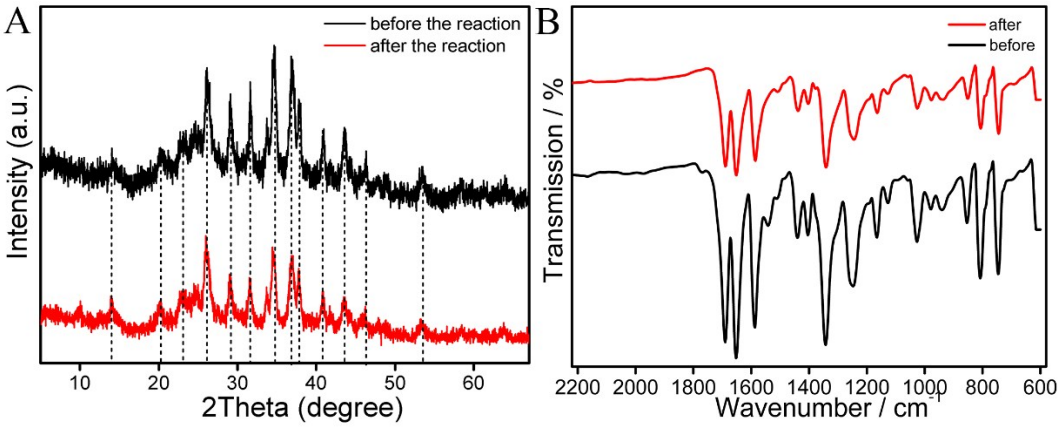

Fig. S8 (A) XRD patterns and (B) FT-IR spectra of the fresh and the used Ag_2S/PDI (1:0.6).

11. The transient fluorescence spectrum

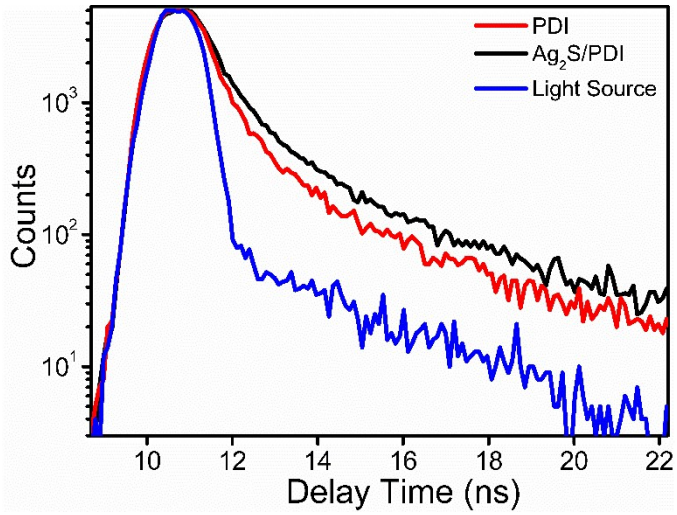

Fig. S9 The time-resolved transient photoluminescence decays spectroscopy for PDI and Ag_2S/PDI (1:0.6), excited at 635 nm.

The lifetime of Ag_2S/PDI was slightly longer than that of pure PDI, indicating that Ag_2S/PDI is more conducive to the separation of h^+-e^- pairs.

12. The electron paramagnetic resonance spectra (ESR) of samples

Figure S10 shows the ESR spectra comparison of PDI and Ag_2S/PDI for detecting $O_2^{\cdot-}$, $^1O_2$ and ·OH, respectively. The results indicate that the composite Ag_2S/PDI can produce more $O_2^{\cdot-}$ and $^1O_2$ than pure PDI. In particular, the content of singlet oxygen in Ag_2S/PDI is about 7 times higher than that in PDI under light. In addition, ESR detected very weak hydroxyl radical signal in both pure PDI and Ag_2S/PDI, which indicated that the hydroxyl radicals were not the dominant active species. The results of ESR are consistent with the free radical trapping experiment.

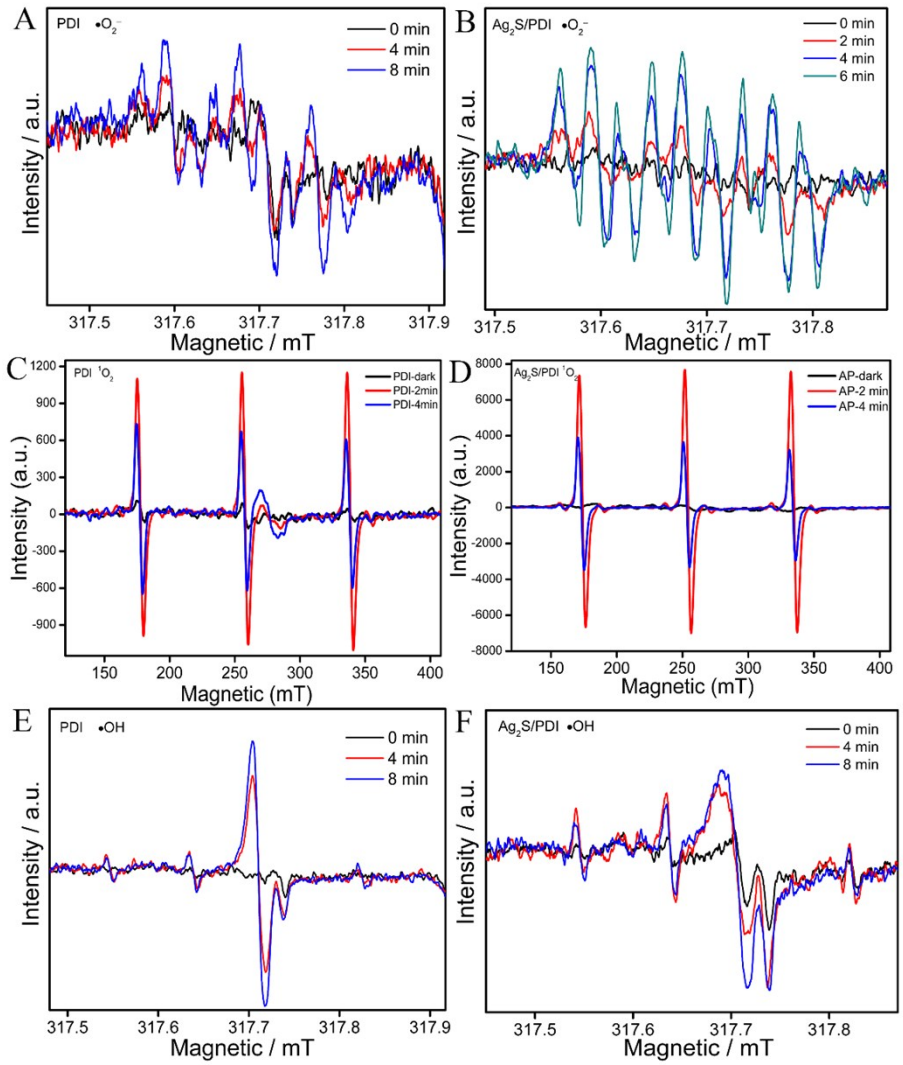

Figure S10 The electron paramagnetic resonance spectra (ESR) of (A) PDI and (B)Ag_2S/PDI in DMSO-methanol for detecting $O_2^{\bullet-}$; (C) PDI and (D) Ag_2S/PDI in TEMP-water for detecting singlet oxygen; (E) PDI and (F) Ag_2S/PDI in DMSO-water for detecting •OH upon irradiation ($\lambda > 420$ nm)

13. Mott–Schottky curves of samples

The flat-band potential of pure PDI obtained from the x intercepts of the linear region in MS plots was found to be −0.24 V versus NHE (Figure S10A). It was reported that the conduction bands of n-type semiconductors are normally 0.1−0.2 eV deeper than the flat-band potential. [10] Herein, the voltage differences between CB value and the flat potential value are set to be 0.1 eV, and thus the bottom of the conduction band of PDI is estimated to be −0.44 eV versus NHE. In addition, the slope of MS spectrum of silver sulfide is less than 1, indicating that silver sulfide is a p-type semiconductor. [15]

The potentials of the conduction band (CB) and valence band (VB) edges of Ag_2S can be obtained according to the Mulliken electronegativity theory, which is shown as follow in Eq. S (1) and Eq. S(2): $E_{VB}= \chi - E_C+0.5Eg$， Eq. S (1)； $E_{CB}=E_{VB}-E_g$, Eq. S (2), where E_{VB} and E_{CB} stand for

the conduction band and valence band edge potential respectively, χ is the absolute electronegativity of the semiconductor, which is the geometric mean of the electronegativities of the constituent atoms, [16] and E_c is the energy of free electrons on the hydrogen scale (about 4.5eV vs NHE), [17] E_g is the band gap of semiconductor. The χ value is calculated to be 4.96 eV for Ag_2S. [18]

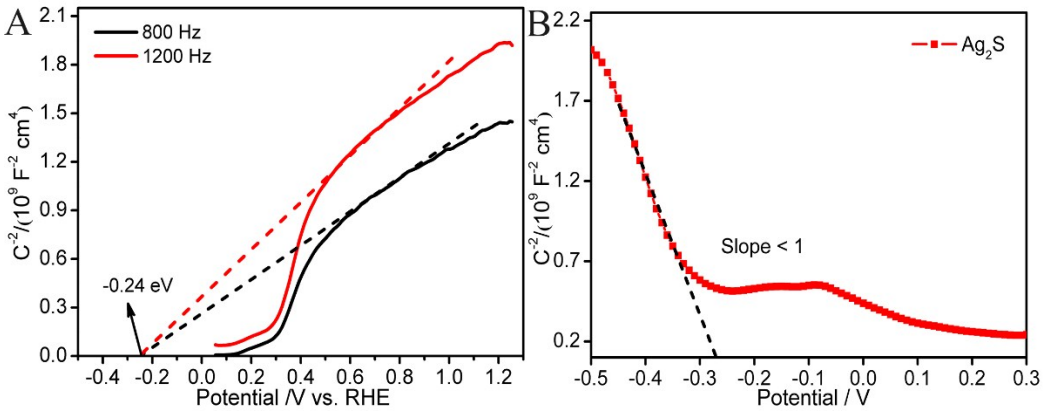

Fig. S11 Mott–Schottky plots of (A) the self-assembled PDI supramolecular and (B) Ag_2S.

REFERENCES:

(1) J. Wang, W. Shi, D. Liu, Z. Zhang, Y. Zhu and D. Wang, *Appl. Catal. B Environ.* 2017,**202**, 289-297.

(2) R. Singh, E. Giussani, M. M. Mróz, F. D. Fonzo, D. Fazzi, J. Cabanillas-González, L. Oldridge, N. Vaenas, A.G. Kontos, P. Falaras, A. C.Grimsdale, J. Jacob, K. Müllen and P. E. Keivanidis, *Organic Electronics,* 2014, **15**, 1347-1361.

(3) J. Yang, H. Miao, Y. Wei, W. Li and Y. Zhu, *Appl. Catal. B Environ.* 2019, **240**, 225-233.

(4) Y. Li, M. Zhang, X. Guo, R. Wen, X. Li, X. Li, S. Li and L. Ma, *Nanoscale Horizons* 2018, **3**, 205-212.

(5) Z. Zhang, J. Long, X. Xie, H. Zhuang, Y. Zhou, H. Lin, R. Yuan, W. Dai, Z. Ding, X. Wang and X. Fu, *Appl. Catal. A Gen.* 2012, **425-426**, 117-124.

(6) J. Yang, R. Hu, W. Meng and Y. Du, *Chem. Commun.* 2016, **52**, 2620-2623.

(7) R. Dong, B. Tian, C. Zeng, T. Li, T. Wang and J. Zhang, *J. Phys. Chem. C* 2012, **117**, 213-220.

(8) F. T. Li, Y. Zhao, Q. Wang, X. J. Wang, Y. J. Hao, R. H. Liu and D. Zhao, *J. Hazard. Mater.* 2015, **283**, 371-381.

(9) T. Yan, M. Sun, H. Liu, T. Wu, X. Liu, Q. Yan, W. Xu and B. Du, *J. Alloys Compd.* 2015, **634**, 223-231.

(10) D. Liu, J. Wang, X. Bai, R. Zong and Y. Zhu, *Adv. Mater.* 2016, **28**, 7284-7290.

(11) C. Zhang and Y. F. Zhu, *Chem. Mater.* 2005, **17**, 3537-3545.

(12) M. Zhang, W. Q. Yao, Y. H. Lv, X. J. Bai, Y. F. Liu, W. J. Jiang and Y. F. Zhu, *J. Mater. Chem. A.* 2014, **2**, 11432-11438.

(13) W. Q. Wei, D. Liu, Z. Wei and Y. F. Zhu, *ACS Catal.* 2017, **7**, 652-663.

(14) Y. Wei, M. Ma, W. Li, J. Yang, H. Miao, Z. Zhang and Y. Zhu, *Appl. Catal. B Environ.* 2018, **238**, 302-308.

(15) R. Bose, G. Manna, S. Jana and N. Pradhan, *Chem. Commun.* 2014, **50**, 3074-3077.

(16) X. Xin, J. Lang, T. Wang, Y. Su, Y. Zhao and X. Wang, *Appl. Catal. B Environ.* 2016, **181**, 197-209.

(17) Y. Su, X. Xin, Y. Wang, T. Wang and X. Wang, *Chem. Commun.* 2014, **50**, 4200-4202.

(18) B. Barrocas, T. J. Entradas, C. D. Nunes and O. C. Monteiro, *Appl. Catal. B Environ.* 2017, **218**, 709-720.